Experiments and Simulations: Enhanced Mechanical Properties of End-Linked Bimodal Elastomers

Geoffrey D. Genesky, Bernardo M. Aguilera-Mercado, Dhananjay M. Bhawe, Fernando A. Escobedo, and Claude Cohen*

School of Chemical and Biomolecular Engineering, Olin Hall, Cornell University, Ithaca, New York 14850

Received May 13, 2008; Revised Manuscript Received July 17, 2008

ABSTRACT: We report on stress−strain and swelling results for polydimethylsiloxane bimodal networks, studied both experimentally and via Monte Carlo simulations. These end-linked networks were formed with negligible extent of soluble fractions, and reasonable agreement is found between experimental results and simulation data. We examine the variation in microstructure for networks with different concentrations of short chains. When the concentration of short chains is low, these chains aggregate during the end-linking process and lead to a heterogeneous network structure, while networks formed with higher short chain concentrations are more homogeneous. Short chains that are long enough to initially have a Gaussian conformation also produce the characteristic stress upturn and enhanced toughness previously reported in bimodal networks with non-Gaussian short chains. We find that it is the limited extensibility of the short chains at high concentrations and not the cluster formation of short chains at low concentrations that leads to the enhanced mechanical properties of these elastomers.

1. Introduction

Bimodal polymer networks consist of two sets of telechelic polymer chains of different molar mass that are chemically identical and end-linked together from the melt state. It has been reported that when such networks are prepared from short and long chains whose molar mass differ by a factor greater than 10, enhanced mechanical properties can result.[1] For example, these bimodal networks can withstand higher loads than long chain unimodal networks without the usual decrease in extensibility found in networks prepared with shorter chains. Therefore, bimodal networks can have both a large ultimate stress and a large ultimate strain. The mechanical enhancement is aided by a characteristic upturn in stress at high strain values. This leads to an improvement in toughness—the energy per unit volume required to rupture the material, which is found by integrating under the stress−elongation ratio curve.

Polydimethylsiloxane (PDMS) is an important component of many silicone elastomers. Its very unique properties, such as low glass transition temperature (−127 °C) and high chain flexibility, make it a rather ideal elastomer to study. The properties of PDMS chains with unimodal chain length distribution end-linked with tetrafunctional cross-linkers have been well characterized.[2−7] For these reasons, and the fact that unimodal PDMS elastomers have been successfully modeled by Monte Carlo simulations,[8−10] we have employed PDMS networks in the present study of bimodal elastomers.

A number of experimental studies of bimodal networks have been previously reported. However, the reasons for the upturn in stress and enhancement in mechanical properties have been debated and are not clear. The two main hypotheses for the improvement in properties are finite extensibility of the short chains, as originally proposed by Mark,[1,11,12] and the clustering of the short chains into heterogeneous structures.[13−17] Mark's experiments used hydroxyl-terminated PDMS chains cross-linked with tetraethyl orthosilicate to create networks with tetrafunctional cross-linking. The short chains always had number-average molar mass (M_n) less than 1100 g/mol, while the long chains were typically about 20 000 g/mol. Mark attributed the increased toughness of bimodal networks to good extensibility due to reapportionment of strain to the long chains during the early stages of deformation, followed by an increase in stress at high elongations due to the limited extensibility of the short chains. However, some researchers have credited the improved properties to heterogeneous domains of short chains in the bimodal networks. Stein et al.[13] used small-angle neutron scattering (SANS) to observe a dramatic increase in the scattered intensity $I(q)$ upon curing of bimodal networks with deuterium-labeled short chains. This observation, along with additional SANS experiments on bimodal networks that showed two characteristic length scales,[14] indicates segregation between the short and long chains. Additional evidence from stress-optical,[15] dynamic light scattering,[16] and nuclear magnetic resonance[17] studies shows that the short chains can segregate into clusters. Proponents of the clustering hypothesis for toughness enhancement envision the smaller chain heterogeneities acting as large multifunctional cross-links similar to the filler particles that are often added to elastomers. Some have theorized that these short chain clusters cause increased toughness through dissipation of elastic energy as the network is deformed.[18]

A number of theoretical studies have also been performed in order to describe the properties of bimodal networks. Several studies have used free energy minimization techniques to generate stress−strain properties. Rotational isomeric state (RIS) or Fixman−Alben distributions were used to describe the end-to-end distances of the chains.[19−23] While these studies are able to describe the short, non-Gaussian chains as they reach their extended state, the network connectivity and resulting interactions between chains are ignored. On the other hand, von Lockette et al.[24] developed a micromechanics-based eight chain model to take into account network connectivity based on a proposed microcomposite arrangement. Each of the eight chains in the model is a "bimodal" chain consisting of a long chain and short chain connected in series with two pairs of cross-links. The model is successful in describing stress−stretch experimental results of Mark's bimodal networks with high concentration of short chains, but it fails to describe others at lower short chain concentrations. The authors speculate that this may be due to the fact that their proposed microcomposite

* To whom correspondence should be addressed.

10.1021/ma801065x CCC: $40.75
Published on Web 10/08/2008

arrangement does not describe all experimental systems. Their model does not incorporate the role of the faster curing kinetics of the much smaller and more mobile short chains.

In this paper, we study the mechanical and swelling properties of bimodal networks in a systematic fashion. We have examined bimodal networks in experimental studies of polydimethylsiloxane elastomers and compared with Monte Carlo simulations mimicking such flexible chains. Several different combinations of short and long chains were employed, including short chains that are long enough to assume a Gaussian distribution of end-to-end vectors when in the unperturbed state. Carefully controlled chemistry has allowed us to create networks with a very low soluble fraction, and these specimens have fewer defects than those employed in many previous experiments. The simulations, unlike much of the previous work, incorporate both the effects of the kinetics of curing networks with two chain length distributions and the presence of entanglements and network connectivity. The agglomeration of short chains is easily monitored in simulation at various bimodal mixture compositions. We compare experimental stress−strain and swelling measurements to Monte Carlo simulations predictions and combine results from experiments and simulations to test the two hypotheses of finite extensibility and nonhomogeneous distribution of short chains that have been used to explain the mechanical improvement seen in bimodal networks.

2. Experimental Procedure

2.1. Synthesis of Precursor Chains. Except for the 800 g/mol chains, which were purchased from Gelest, Inc., PDMS precursor chains were synthesized via an anionic ring-opening polymerization from hexamethylcyclotrisiloxane monomer[25,26] (Gelest, Inc.). The monomer was dissolved in 50 wt % toluene, and an empirically determined amount of HPLC water was added to control the molecular weight of the resulting polymer. After heating the solution to 60 °C, the reaction began with the addition of benzyltrimethylammonium bis(*o*-phenylenedioxy)phenylsiliconate catalyst and dimethyl sulfoxide promoter. After 2 h the reaction was complete, and the mixture of toluene and PDMS chains was allowed to cool to room temperature. Addition of an excess of pyridine (an acid scavenger) and vinyldimethylchlorosilane converted the PDMS chain ends to vinyl groups. The polymer chains were then washed with water and precipitated in a mixture of toluene and methanol. Any remaining solvent was removed by drying in an oven for 3 days.

The molar mass distributions were characterized by gel permeation chromatography (GPC). The columns were calibrated using polystyrene standards with narrow polydispersity, and equivalent PDMS molar masses were obtained using a well-established conversion.[27] For the 800, 4500, 10 000, 21 000, 29 000, and 91 000 number-average molar mass chains used in this study, the corresponding polydispersity indexes were 1.43, 1.18, 1.33, 1.25, 1.27, and 1.38.

2.2. Synthesis of PDMS Bimodal Networks. For the bimodal networks studied here, the mole percentage of short chains was varied from 60 to 98%. The total mass of short chains required was calculated using

$$g_{\text{short}} = g_{\text{total}}\left[\frac{x_{\text{short}}M_{\text{n,short}}}{x_{\text{short}}M_{\text{n,short}} + x_{\text{long}}M_{\text{n,long}}}\right] \quad (1)$$

Here, g is the mass in grams, M_n is the number-averaged molar mass in g/mol, and x is the mole fraction. The short chain and long chains masses were measured and combined. Next, the necessary volume of tetrakis(dimethylsiloxy)silane cross-linker ($\mu L_{\text{cross-linker}}$) (Gelest, Inc.) was calculated using

$$\mu L_{\text{cross-linker}} = 185916r\left[\frac{g_{\text{short}}}{M_{\text{n,short}}} + \frac{g_{\text{long}}}{M_{\text{n,long}}}\right] \quad (2)$$

In this equation, the prefactor 185916 (in μL/mol) is calculated from the density and molar mass of the cross-linker to balance the number of reactive ends of the tetrafunctional cross-linker with chain ends of the difunctional PDMS. We define a parameter r to represent the ratio of cross-linker arms to polymer chain ends such that $r = 1$ represents a stoichiometric balance between the two. Past work has shown that $r = 1.7$ yields the highest quality unimodal networks[2] when the precursor chains have molar masses greater than 10 000. Therefore, $r = 1.7$ was used to produce optimal (low soluble fractions) long chain unimodal networks. Other researchers have demonstrated that the highest quality short chain unimodal networks are formed at lower r ratios.[28] Thus, bimodal networks with 800 g/mol short chains required less cross-linker to produce optimal networks, so r was reduced to 1.1 as the mol % of short chains increased. For the 4500−91 000 M_n bimodal network series, $r = 1.7$ was used for both the long chain unimodal and the bimodal networks.

After the short chain, long chain, and cross-linker were added, they were well-mixed with a spatula and placed on a rotator overnight to ensure homogeneity. The catalyst for the network formation, *cis*-dichlorobis(diethylsulfide)platinum(II), was dissolved in a minimal amount of toluene and then mixed into the PDMS and cross-linker. After transfer to Teflon molds, the networks were cured at 35 °C for 3 days.

2.3. Mechanical Testing to Fracture in Extension. After the networks were cured, they were removed from the molds, and a sample puncher was employed to produce test pieces of uniform width and thickness. Typical samples were 0.5−1 mm thick and 4.3 mm wide. The distance between the two clamps was 40−45 mm. We measured engineering stress (force/initial cross-sectional area) versus extension ratio (length/initial length) with an Instron uniaxial extension setup. The samples were clamped in their undeformed state at room temperature and extended at 20 mm/min until fracture. This strain rate was selected after verifying that the stress−strain data were independent of strain rate at this slow extension speed. Young's modulus (E) was determined by calculating the slope of the best fit line through the first 5% of the stress−strain curve, where the trend is linear.

3. Simulation Procedure

3.1. Network Formation. Simulations of the cross-linking reaction leading to network formation were carried out on a lattice using the bond fluctuation model (BFM).[29,30] This coarse-grained lattice algorithm is simple enough to allow a complete and simultaneous analysis of both static and dynamic quantities.[31] For this reason the BFM has been widely used in simulation studies of structural properties of polymer networks.[8,32−35] In this framework, coarse-grained chain monomers and cross-linking species were modeled as cubes occupying 8 lattice points and capable of forming bonds along any of 108 distinct bond vectors. The geometric constraints in this model disallow the crossing of chains. Chains and cross-linking species were first inserted in the simulation box and then relaxed using hop moves that resemble diffusive dynamics.[8,31,32] The network formation process is carried out athermally, i.e., taking into account excluded volume interactions and bonding restrictions only. Thus, the displacement moves are accepted if the new lattices positions are unoccupied and the new bond vectors belong to the set of available bond vectors in the BFM. The fraction of occupied lattice points was set at $\phi = 0.46-0.47$, a value that has been shown to represent meltlike conditions.[36]

After equilibration (up to 10^6 moves per repeat unit, a number greater than the one used in previous works[32]), the end-linking reaction was turned on by allowing bonds to form between nearest-neighbor chain ends and tetrafunctional cross-linkers, while the system continued being relaxed by the hop moves. Any such reactive sites coming in "contact" reacted with 100% probability to speed up the cure rate of the network without affecting the structural evolution of the soluble fraction or the

Table 1. Description of the Simulated 15−300 Network Series

short chain content (mol %)	r	number of short chains	number of long chains	number of cross-linkers
100	1.05	2650	0	1391
95	1.10	778	41	451
90	1.05	490	54	286
60	1.15	110	73	105
0	1.20	0	80	48

network imperfections during the cure.[35] The reaction was run until the percentage of unreacted chain ends was 1% or lower. The value of the parameter r (ratio of cross-linker arms to chain ends) used for each simulated system was optimized to obtain low soluble fractions (based on preliminary runs where r was varied over the $1.0 < r < 1.2$ range). These optimized r values were significantly lower (around 30%) than the ones used in experiments. This is because the simulated end-linking reaction in the framework of the BFM yields more ideal networks in terms of the soluble fraction compared to experiment.[35] In experimental networks a considerable part of the cross-linkers may not react completely with the chain ends due to side reactions and steric hindrances.[32,37]

The characteristics of the simulated 15−300 networks corresponding roughly to the experimental 4500−91000 M_n systems are shown in Table 1. Because of the large system sizes involved, finite size effects were assessed for selected systems only (e.g., for the pure short chain networks for which elastic properties were found to be unchanged for systems with sizes varying by a factor of 2). Such effects are expected to be more strongly reflected in the properties of the long chains because the sizes of the simulation boxes were typically just a few times a multiple of the long chain end-to-end distances. For consistency, the size of all simulated networks was chosen to be similar to allow for a meaningful *qualitative* comparison of the properties among the different networks.

3.2. Network Deformation. Uniaxial deformations were implemented off-lattice to allow for continuous dimensional changes of the simulation box. The coordinates from the BFM lattice were transformed into the off-lattice framework to preserve the polymer volume fraction and the network structure. Both the monomers along the chain and the cross-linkers were modeled as spherical beads of diameter σ_{LJ} and interaction energy of ε_{LJ}. The bond length was allowed to fluctuate to within $\sigma_{LJ} \pm 0.2\sigma_{LJ}$. Nonbonded beads interact via a cut-shifted Lennard-Jones potential cutoff at $r_c = 2^{1/6}\sigma_{LJ}$. The interbead interaction was thus purely repulsive. In order to prevent bond crossing, a bead−bead overlap distance was set ($r_o = 0.85\sigma_{LJ}$), below which the repulsive bead−bead interaction energy is infinite.

Hop, flip, and cluster MC volume moves—in random order—were used to relax the system in a physical pseudodynamic way. These moves were grouped in MC cycles, where one cycle roughly mimicked one molecular dynamics step. In a hop move a single bead is translated a small random distance in a random direction; in a flip move a single bead is rotated a random angle around the axis formed by the line joining the centers of its two neighbor bonded sites; in a cluster volume move the simulation box volume (along one or more selected axes) is varied while preserving the network internal topology.[8,38] Detailed Metropolis acceptance rules for these moves are given elsewhere.[38] One MC cycle includes a fixed number (usually equal to the number of beads in the system) of attempted single-site moves (95% hops and 5% flips) and one or two volume moves.[8,33] The acceptance ratios for the volume and single site moves were 0.45 and 0.17, respectively. Isotropic (box-shape preserving) NPT simulations at $P = 3.0$ (in units of k_BT/σ_{LJ}^3) and at $T = 2.0$ (in units of ε_{LJ}/k_B) were used to initially equilibrate the system at a meltlike density. Extension simulations were subsequently performed in an isostress ensemble. The imposed stress was calculated from $\sigma = (P_{xx} + P_{yy})/2 - P_{zz}$, and the extension ratio was taken as the ratio of the box z length after the stress is imposed to the initial box z length, where P_{xx}, P_{yy}, and P_{zz} are the applied pressures in the x, y, and z directions, respectively. Up to 10^7 MC cycles were simulated to achieve mechanical equilibrium at any given stress value. The system was assumed to be in equilibrium when the dimensions of the simulation box reached plateau values that remained constant (within statistical fluctuations) for $\sim 10^6$ cycles. Typically, a system equilibrated at a particular stress value was used as a starting point for the simulation at the next higher stress value. The order parameters for both the short and long chain segments were calculated from the expression $S = \langle(3\cos^2\theta - 1)/2\rangle$, where θ is the angle between a given segment and the strain axis. Equilibrium swelling calculations were performed with an implicit solvent in the NPT ensemble and $P^* = 0$.[8]

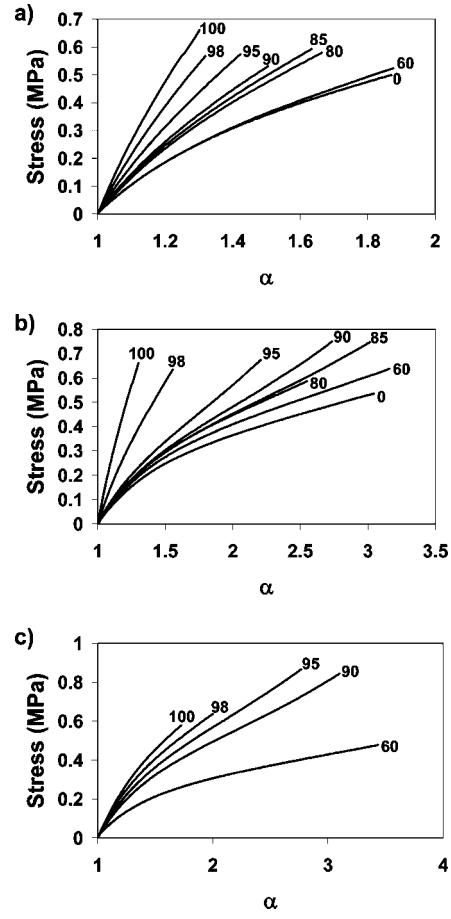

Figure 1. Engineering stress f/A^* (force divided by initial cross-sectional area) versus extension ratio α for bimodal networks (a) 800−10 000 g/mol networks, (b) 800−29 000 g/mol networks, and (c) 4500−91 000 g/mol networks. Curves are labeled with mol % short chains.

4. Experimental Results and Discussion

4.1. Stress−Elongation Results. Experimental stress−extension ratio data curves up to network rupture for three series of bimodal networks are presented in Figure 1. The area under each curve is the energy needed to break the network, which is known as the toughness of the elastomer. Toughness values, other mechanical and swelling properties, and the swelling ratio Q are listed in Table 2.

Each sample produced 4−6 test pieces. While the stress−strain curve was reproducible from sample to sample, inherent flaws

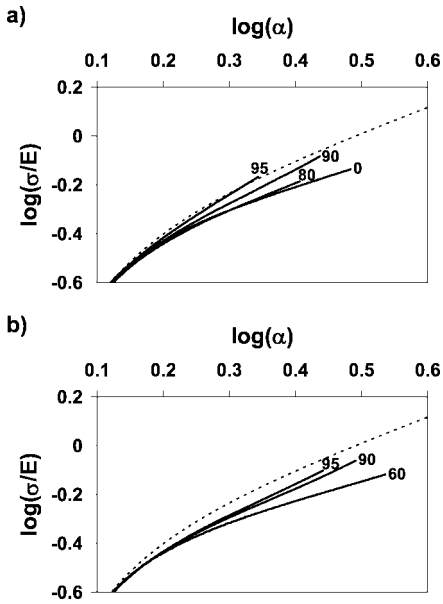

Figure 2. Logarithmic plot of engineering stress normalized by modulus versus extension ratio for bimodal networks (a) 800−29 000 g/mol networks and (b) 4500−91 000 g/mol networks. Curves are labeled with mol % short chains. Dashed line represents ideal rubber elasticity (eq 3), which is based on the assumption of affine deformation.

in the test pieces caused variations in the breaking points. Therefore, we have presented the average and standard deviation for the modulus, toughness, and ultimate stress data. A few samples broke prematurely near one of their edges due to the clamping force and were not included in this statistical analysis. Since presenting all of our data in Figures 1−5 would be too cluttered, we have chosen to show the data of the test pieces that reached the highest elongation ratios in these plots.

Some tests in uniaxial extension with a precut to concentrate the stress were attempted, but though the same trends were observed, we still found a comparable amount of scatter in these experiments. We have recently obtained consistent results for tear energies from precut samples in the "pure shear" geometry.[39] We will report these results in a forthcoming publication.[40]

4.2. Toughness. For the 800−10 000 g/mol series (Figure 1a), no toughness enhancement was seen. The 60 mol % short chain network performs similarly to the unimodal 10 000 g/mol samples. At higher concentration of short chains, the networks do not exhibit an upturn in stress at high elongations and do not show improved toughness. The only effect of bimodality here seems to be to tune the elastic modulus (E). We note that the ratio of molar masses in this bimodal system has only a moderate value of 12.5.

With a short chain of 800 g/mol and a long chain of 29 000 g/mol (Figure 1b), however, some of the bimodal networks have better toughness than their unimodal counterparts. When the short chain concentration is 85−95 mol %, the stress is seen to upturn before rupture. The 85 mol % short chain network seems to give the best combination of elongation, ultimate stress, and toughness. Comparison to the performance of 800−10 000 g/mol networks suggests that the greatest enhancements in mechanical properties are seen when the molar masses of the precursor chains are quite widely separated.

While the improvement in toughness can clearly be seen in 800−29 000 M_n networks, it is only of the order of 25−50%. This enhancement is less than previously reported. This can be attributed to the fact that we are able to make "optimal" 29 000 g/mol networks that leads to a very low soluble fraction (w_{sol}) and few inelastic chains. Previous researchers used a stoichiometric amount of cross-linker corresponding to $r = 1.0$ for both bimodal and unimodal networks. Since the optimal r for these bimodal samples at 85−95 mol % is about 1.1 due to the large amount of short chain ends, older work had fortuitously employed bimodal networks of higher quality than the unimodal networks they were being compared to. Here, we were able to prepare all networks as close to defect-free as possible, as evidenced by soluble fraction values of 1.07% or less for samples in the 800−10 000 and 800−29 000 M_n series.

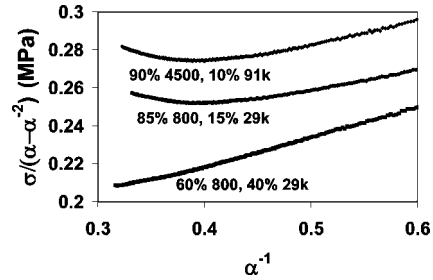

Figure 3. Reduced stress vs inverse elongation for three bimodal networks. Those at 85−90 mol % short chains show a clear upturn in stress, while 60% does not. The curve for 60 mol % 4500, 40 mol % 91 000 shows a similar line shape to the 60 mol % curve above.

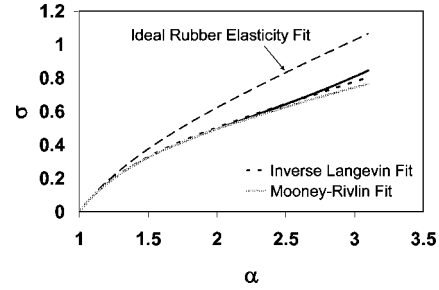

Figure 4. Ideal rubber elasticity, inverse Langevin, and Mooney−Rivlin fits to the stress−elongation ratio curve for the 90% 4500−10% 91 000 g/mol bimodal network. The experimental data are represented by the solid line. The inverse Langevin equation fit yields a characteristic strand length in between the long and short chain molecular weights.

4.3. Stress Upturn. Examination of the stress−strain performance of bimodal networks with short chains of molar mass 4500 g/mol also reveals stress upturns at high strains. Therefore, enhanced mechanical properties in bimodal networks cannot be solely attributed to the presence of very short chains that are non-Gaussian in the undeformed state. Because the long chain component (91 000 g/mol) contains so few chain ends, it is difficult to completely end-link a pure long chain melt or mixtures with low % short chains in a reasonable cure time. As shown in Table 2, the 60 mol % short chain network in this series had a soluble fraction of 3.74%.

It is instructive to normalize the stress σ by the elastic modulus E, as plotted in Figure 2 for the 800−29 000 and 4500−91 000 M_n bimodal systems. This allows comparison to the model of ideal rubber elasticity:

$$\frac{\sigma}{E} = \frac{\alpha - \alpha^{-2}}{3} \tag{3}$$

For both systems, all curves initially follow the ideal model (the dashed curve) but deviate downward as α increases. This expected behavior for elastomers is usually attributed to the presence of entanglements (often associated with the C_2 term in the Mooney−Rivlin representation).

However, due to non-Gaussian behavior and limited extensibility at large values of α, some of the experimental curves

Table 2. Bimodal Network Compositions and Properties[a]

M_n (g/mol) of short chains	M_n (g/mol) of long chains	mol %, mass % of short chains	E (MPa)	Q	w_{sol} (mass %)	toughness (MPa)	ultimate stress (MPa)
800	10 000	0	1.04 ± 0.03	3.16	0.34	0.20 ± 0.06	0.44 ± 0.06
		60,11	1.06 ± 0.02	3.16	0.49	0.17 ± 0.08	0.43 ± 0.08
		80,24	1.33 ± 0.02	2.74	0.76	0.16 ± 0.05	0.50 ± 0.07
		85,31	1.38 ± 0.03	2.73	0.73	0.15 ± 0.06	0.49 ± 0.09
		90,42	1.46 ± 0.03	2.67	1.02	0.10 ± 0.04	0.44 ± 0.07
		95,60	1.74 ± 0.03	2.44	0.70	0.08 ± 0.04	0.45 ± 0.09
		98,80	2.14 ± 0.11	2.30	1.07	0.07 ± 0.02	0.47 ± 0.07
		100	2.72 ± 0.11	2.06	0.90	0.09 ± 0.02	0.59 ± 0.10
800	29 000	0	0.74 ± 0.04	3.75	0.78	0.53 ± 0.12	0.48 ± 0.04
		60, 4	0.82 ± 0.04	3.57	0.71	0.51 ± 0.24	0.51 ± 0.09
		80,10	0.89 ± 0.02	3.53	0.36	0.44 ± 0.12	0.53 ± 0.05
		85,14	0.88 ± 0.02	3.54	0.38	0.85 ± 0.03	0.74 ± 0.01
		90,20	0.88 ± 0.03	3.47	0.90	0.63 ± 0.14	0.68 ± 0.09
		95,34	0.95 ± 0.04	3.10	0.49	0.37 ± 0.08	0.60 ± 0.06
		98,57	1.43 ± 0.03	2.66	0.88	0.15 ± 0.03	0.57 ± 0.10
		100	2.72 ± 0.11	2.06	0.90	0.09 ± 0.02	0.59 ± 0.10
4500	91 000	60, 7	0.64 ± 0.03	5.17	3.74	0.64 ± 0.10	0.45 ± 0.02
		90,31	0.94 ± 0.01	3.62	0.26	0.90 ± 0.09	0.79 ± 0.04
		95,48	1.09 ± 0.03	3.40	0.22	0.79 ± 0.09	0.82 ± 0.04
		98,71	1.24 ± 0.04	3.15	1.00	0.28 ± 0.09	0.57 ± 0.07
		100	1.34 ± 0.06	3.06	0.93	0.24 ± 0.01	0.57 ± 0.02

[a] Modulus, toughness, and ultimate stress values reported are the average and standard deviation of 4−6 test pieces.

Table 3. Chain Extensions for Unimodal and Bimodal Networks

component	mol %	M_n (g/mol)	r_m (Å)	α upturn	r upturn (Å)	r/r_m upturn	α fracture	r fracture (Å)	r/r_m fracture
unimodal	unimodal	4 500	163				1.73	85	0.52
		10 000	362				1.87	137	0.38
		21 000	761				2.01	213	0.28
		29 000	1050				3.05	379	0.36
short chain	60	4 500	163				3.43	168	1.03
long chain	40	91 000	3296				3.43	756	0.23
short chain	90	4 500	163	2.57	126	0.77	3.10	152	0.93
long chain	10	91 000	3296	2.57	566	0.17	3.10	683	0.21

exhibit an upturn in stress seen at higher concentrations of short chains. These curves again approach the ideal rubber elasticity values of σ/E once they are stretched far enough. In fact, the data of the 95 mol % 800−5 mol % 29 000 network slightly overtake the ideal curve. Thus, the presence of the short chains appears to mitigate the effect of the "slippage" of entanglements on the stress−stretch curve as the strain increases.

Plotting the data in a Mooney−Rivlin representation is a better way to visualize the upturns in stress. This is done by dividing the engineering stress by $\alpha - \alpha^{-2}$ and plotting the results against α^{-1}. Some curves of interest are shown in Figure 3. It is evident that networks of 85 and 90 mol % short chains show a clear upturn in stress at high elongation ratios. This is seen at inverse elongation values of less than about 0.4. The curve for the 60% short chain network, however, does not display an upturn.

If we consider the bimodal network of 90 mol % short chains of 4500 g/mol with long chains of 91 000 g/mol, both chains are Gaussian in their unperturbed state. It may then be instructive to perform a simple calculation of the affine extension of both chains even though it has been established that affine deformation does not hold all the way down to the macromolecular scale in elastomers. The maximum extensibility of a PDMS chain r_m as a function of number of monomer units n has been shown to be[41]

$$r_m = 1.34n = 1.34(2M_n/74) \quad (4)$$

The prefactor, 1.34 Å, is the axial length of a PDMS bond in its most extended state, and 74 g/mol is the molar mass of an $Si(CH_3)_2$−O unit. Additionally, the average chain extension r at elongation ratio α for a PDMS chain of a given M_n can be calculated based on affine deformation from the relation[42]

$$r = \langle r_0^2 \rangle^{1/2}\alpha = 730 \times 10^{-3}(M_n)^{1/2}\alpha \quad (5)$$

Here, r_0 is the unperturbed end-to-end distance of a PDMS chain and the prefactor 730×10^{-3} has units of Å $mol^{1/2}$ $g^{-1/2}$.

Use of these relations provides a simple way to calculate the extension ratio of each chain compared to its maximum extension (r/r_m). Therefore, the reduced stress−inverse elongation plots in Figure 3 allow us to determine the elongation at which the stress rise occurs for a given network. Calculations of the extension of each chain at both the stress upturn and the network rupture are given for some unimodal and bimodal networks in Table 3 assuming affine deformation. The unimodal end-linked networks and the 60 mol % short chain 4500−91 000 M_n network lack an upturn in stress at high extension ratios. However, once the short chain mol % is increased to 90%, the stress does increase rapidly before fracture of the network. For the unimodal networks shown in Table 3, the affine deformation calculation of r/r_m predicts that the end-linked chains are at about 30−50% of their maximum extensibilities at fracture. However, the bimodal networks stretch to much higher elongation ratios. According to this crude calculation, the synergistic effect of the two chain length distributions results in the short (4500 g/mol) chains stretching to their maximum lengths in the bimodal systems. More reliable estimates of r/r_m have been obtained from simulations and are presented later (Figure 9). One can also argue against affine deformation of the short chains in the case of low molar fractions of short chains in the bimodal networks because of strong evidence of short chain cluster formation. In these inhomogeneous bimodal networks, the load is not evenly distributed across the network.

We have also attempted to take into account the physical phenomena that cause deviations from the ideal rubber elasticity results shown in Figure 2. At moderate extension, the deviation

can be assumed to be due to the slippage of entanglements leading to a reduction of the stress from its ideal rubber elasticity value. At higher elongation limited extensibility takes over, and the stress starts to increase again. A semiempirical approach that accounts for both effects is to combine the Mooney−Rivlin representation[43,44] with the inverse Langevin expression for non-Gaussian chain deformation.[45] We could then write

$$\sigma = \frac{2C_1}{3}n^{1/2}\left[L^{-1}\left(\frac{\alpha}{n^{1/2}}\right) - \alpha^{-3/2}L^{-1}\left(\frac{1}{\alpha^{1/2}n^{1/2}}\right)\right] + \frac{2C_2}{\alpha}(\alpha - \alpha^{-2}) \quad (6)$$

where C_1 and C_2 are the Mooney−Rivlin coefficients and L^{-1} is the inverse Langevin expression. This combination would in principle make the equation applicable at low, medium, and high elongation ratios.[46] Equation 6 has been used previously by Meissner[47] on some of Mark et al.'s data on bimodal networks.[1,11] The parameters C_1 and C_2 can be determined from the data up to moderate extension ratios, and the values for stress and elongation ratio at the upturn can be used in eq 6 to determine n. This calculation yields $n = 105$ for 90 mol % short chains in the 4500−91 000 g/mol bimodal network. This corresponds to a PDMS molar mass of about 30 000 g/mol. Therefore, the characteristic elastic strand length at the upturn location is much longer than the short chain length but much shorter than the long chain component. This supports the idea that at this high concentration of short chains the network is more homogeneous and the load (stress) is more uniformly distributed.

The experimental data for this bimodal network are shown Figure 4 in comparison with the ideal rubber elasticity expression (eq 3), the Mooney−Rivlin equation, and eq 6 with $n = 105$. As expected, the ideal rubber elasticity (one-parameter fit) gives a good fit only at low extension ratios. The Mooney−Rivlin equation (two-parameter fit) gives a good fit up to moderate extension ratios but fails at high extension. Equation 6 with three parameters gives a good fit up to the point where the stress upturn occurs. However, at network rupture the maximum stress is about 5% higher than that predicted by eq 6. Therefore, the upturn itself is not completely described by this equivalent "unimodal" network of 30 000 g/mol elastic chains, but instead by a shorter length scale. Nonetheless, as compared to the result of the 60 mol % short chains, this result indicates a better sharing of the load between the two chains of this bimodal network of 90 mol % short chains.

5. Comparison to Monte Carlo Simulations

5.1. Stress−Elongation and Swelling Results. Monte Carlo simulations and experimental results can be compared by obtaining the equivalent molar mass of a simulation bead. This is done by comparing the entanglement molecular weight observed experimentally for PDMS[48] to the number of beads in chains that exhibit entanglements in simulation.[49] A conversion factor of 300 g/mol per LJ bead is obtained.

The short and long chains employed in Monte Carlo studies of bimodal networks were 4 and 69 LJ beads and 15 and 300 LJ beads. Using the conversion above, these correspond to bimodals networks of 1200−20 700 and 4500−90 000 g/mol, respectively. We have experimentally examined the properties of bimodal networks formed from chain mixtures of 800−21 000 and 4500−91 000 g/mol, which can readily be compared to the 4−69 and 15−300 bead simulated systems. Some of the plots comparing the 4−69 bead and 800−21 000 g/mol networks have been included in the Supporting Information.

The equivalence between the nondimensional simulated stress, σ_{sim}, and the experimental dimensional stress, σ_{exp}, is given by

$$\sigma_{sim}k_bT/\sigma_{LJ}^3 = \sigma_{exp} \quad (7)$$

where σ_{LJ} is the Lennard-Jones bead size and k_bT has its usual meaning. To compare experiments with simulations, the data from the 4500−91 000 g/mol bimodal networks were fit to the 15−300 bead data in the low strain region. After plugging in the pertinent values for k_b and room temperature, the fits yielded an average value of $\sigma_{LJ} \approx 7.15 \times 10^{-10}$ m. While the pervaded volume of a bead representing 4 PDMS repeat units is difficult to predict, this value certainly seems reasonable, given that the Si−O bond length is ∼1.63 Å.[50,51] Figure 5 shows the comparison between experimental and simulation results of the stress−elongation ratio data. Although there is some divergence as the networks are stretched to higher extensions, the simulations and experiments show rather good agreement. The largest deviations in the data result from a slight overprediction of the stress upturn in bimodal networks by the Monte Carlo simulation. We note that while the end points of the experimental curves represent breakage points, the simulation does not have a bond-breaking mechanism built in. Molecular dynamics simulations are currently being investigated to achieve fracture. The stress−extension ratio curves for the 4−69 systems showed similar trends as in Figure 5, but the simulation data tended to deviate more from the experimental measurement for bimodals with high concentration of short chains. We suspect that this could be due to the stiffness of the 4-bead simulated chain and its inability to represent the flexibility of the experimental 800 g/mol chain. This discrepancy is also reflected in the extent of swelling of these networks discussed below.

An interesting result of Figure 5 is the similarity between the pure long chain (0% short chain) and 60 mol % short chain curves in the 15−300 bead, simulated system. Note that the unimodal long chain network is not shown for the experimental series. At relatively high molecular weights like 91 000, it is impossible to end-link into unimodal networks of "model" quality because of the increased soluble fraction (and therefore also network defects). However, Figure 1a,b demonstrates that a similar matching is observed in experimental systems as well. This similarity between the 0 and 60 mol % short chain networks is also reflected in the equilibrium swelling of the networks in a solvent.

The PDMS networks were swollen in toluene, and the equilibrium volume fraction of the polymer Φ_0 was determined using standard gravimetric procedures.[52] The equilibrium swelling calculations in simulation were done with an implicit solvent. Since the simulations were not done with an interacting solvent, the simulated networks swell more than the corresponding experimental networks (leading to lower simulated Φ_0 values).[8] Therefore, the data of each simulated series are shifted upward to match the corresponding experimental Φ_0 values of a unimodal network (4500 and 21 000 g/mol) to allow for simple comparison. The matches to unimodal 4500 and 21 000 g/mol networks were chosen because of limitations of the 4-bead representation of the 800 g/mol chains on one hand and the experimental difficulty of synthesizing low soluble fraction 91 000 g/mol networks on the other hand.

The most striking result of Figure 6 is the fact that the 0 and 60 mol % short chain networks have very similar Φ_0 values (i.e., very similar extent of swelling for both experimental data and simulation results). Thus, despite the addition of the short chains (and a cross-link density over 2 times greater in the 15−300 case), the overall response to swelling of each of these networks appears to be quite similar. The simulation data of the 15−300 series match with experimental results of the equivalent experimental bimodal networks quite well (just as for the stress in Figure 5). However, the 4−69 networks swell a lot less than the corresponding experimental bimodals at high

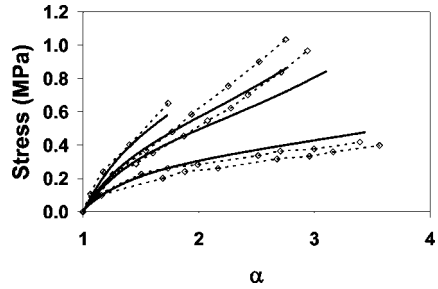

Figure 5. Comparison of 4500−91 000 g/mol experimental stress−elongation ratio curves (solid lines) with 15−300 bead networks from simulation (dashed lines). The curves correspond to 100, 95, 90, and 60 mol % short chain with decreasing modulus for both simulation and experiment. The lowest modulus dashed curve is a 300 bead unimodal network.

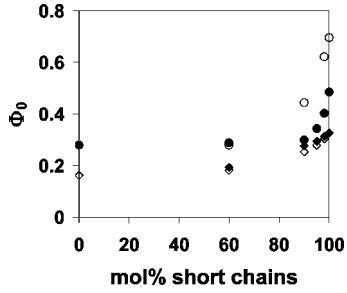

Figure 6. Polymer volume fraction when swollen (Φ_0) vs mol % short chains for the experimental (filled symbols) and simulated (open symbols) networks. Circles represent 4−69 networks and their experimental analogue, while diamonds correspond to 15−300. Note the similar degree of swelling for the 0 and 60 mol % short chain networks. The disparity in Φ_0 values is explained in the text.

concentration of short chains after normalizing the data to the experimental unimodal long chain network. This is consistent with the deviations between simulation results and experimental measurements of stress−strain data of these systems mentioned earlier.

5.2. Microstructure of Bimodal Networks. *5.2.1. Clustering of Short Chains.* At 60 mol % short chains, the majority of the chain ends in the system come from the short chains, but due to the large difference in chain lengths, most of the volume of the system is occupied by the long chains. At this volume fraction of short chains, their concentration is below their overlap concentration. One would then expect a heterogeneous distribution of short chains due to the faster curing kinetics of the much smaller chains. When the short chain concentration is increased, there are many more chain ends available, and a percolated network of short chains with interspersed long chains should result.

This phenomenon is illustrated by calculating the number of chains contained in the pervaded volume of one long chain. By accounting for the chain stiffness and density values for a Gaussian PDMS chain, it can be shown that

$$N = 0.0387 M_n^{1/2} \quad (8)$$

Here, N represents the number of chains contained in the volume occupied by one long chain. Therefore, while a unimodal long chain network in the 4−69 series would contain ∼5.5 total chains in its pervaded volume, it will clearly contain many more short chains in bimodal mixtures. This is illustrated in Figure 7 for a bimodal mixture of Gaussian chains with a molar mass ratio of 18. These cartoons show that the short chains begin to overlap as their concentration increases.

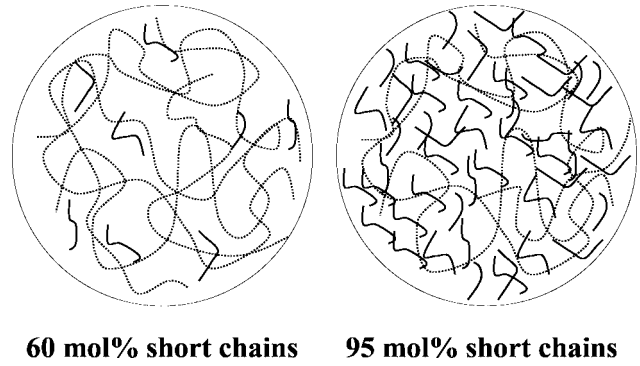

Figure 7. Sketches of short chains (solid) and long chains (dashed) contained in the pervaded volume of a long chain of a bimodal mixture with molar mass ratio of 18.

The degree of clustering in the network is demonstrated by comparing the computer-simulated intermolecular pair distribution function [$g(r)$] of the short chain centers of mass from before the cross-linking reaction to after the reaction is complete. Here, r is in units of bead diameters. A clustered network should have an increased $g(r)$ over the length scale on order of the short chain radius of gyration. Figure 8a demonstrates the short chains clustering in a 60 mol % short chain network as the cross-linking proceeds. The pair distribution function increases with time and then eventually becomes stable when the short chain ends have all reacted.

The ratio of $g(r)$ of the cured state to the original $g(r)$ of the melt state is thus greatly increased over unity for the 60 mol % short chain networks. As shown in Figure 8b, any increase in this ratio is much less pronounced for 90 and 95 mol % short chain networks. This supports the representation of a bimodal network with high short chain content as a network with a relatively homogeneous distribution of short chains throughout the network.

A microstructure of heterogeneous domains of the short chains at 60 mol % helps to explain the results of Figure 6. While the cross-link density is markedly increased when moving from 0 to 60 mol % short chains, macroscopic swelling of the networks in experiments and in simulations is similar. Swelling within these densely cross-linked clusters that occupy only 7% of the total volume (Table 2) is limited, and therefore the overall swelling is almost solely dictated by the changes in the microstructure of the long chains. This seems consistent with the results of Sommer and Lay,[53] who have simulated the swelling of bimodal networks using the bond-fluctuation model. They find that the global swelling ratio is caused by the unfolding of substructures of interconnected short chains linked by long chains that unfold in nonaffine deformation.

As seen in Figure 8, the clustering phenomenon appears to be much more important at lower mol % short chains. Furthermore, as reported in Figures 5 and 6, there is little to no enhancement in the mechanical properties of these dilute short chain bimodal networks. Thus, it appears that these small, heterogeneous clusters of short chains do little to reinforce the elastomers. An examination of past experimental works that demonstrated heterogeneities and clustering of short chains shows that they were carried out at relatively low short chain concentrations. For instance, Stein et al.[13] performed SANS measurements on PTHF bimodal networks with 50 and 70 mol % deuterated short chains of molar mass 1000 g/mol with hydrogenated long chains of molar mass 10 000 g/mol. Hecht et al.[14] also reported short chain aggregation in a bimodal network of 68 mol % short chains. Additionally, these authors did not report the mechanical properties of these networks. Given our findings, we suspect that these clustered short chain

networks would not have demonstrated enhanced mechanical properties.

It is interesting to note that the bimodal networks with the best experimentally determined ultimate properties contain an amount of short chains around their overlap concentration. For example, we can calculate the point at which the short chains begin to overlap in the 15−300 series using the expression for the radius of gyration R_g of an ideal chain. For $N = 15$, overlap occurs at short chain volume fraction 0.47, which corresponds to 95 mol % in this system. Examination of Table 2 shows that for a corresponding 4500−91 000 M_n system 90 and 95 mol % short chain networks give optimum toughness. We note that the simulation results shown in Figure 8b suggest that some degree of clustering may be present even at these high concentrations of short chains. This is also supported by the presence of bimodality in the distribution of residual dipole−dipole coupling as measured by multiple-quantum NMR for bimodal systems of 780−47 200 g/mol.[17] It thus appears that this intermediate structure between prevalent cluster formation at low concentration of short chains and homogeneous distribution at very high concentration leads to the best ultimate mechanical properties of bimodal networks.

5.2.2. Chain Deformation under Extension. Our Monte Carlo simulations provide insight into the possible microstructure of bimodal networks at different concentrations of short chains. Both chain deformation and order parameter were monitored for the short and long chains as the networks were strained. Chain deformation is represented by the ratio of the average chain end-to-end distance ($\langle r_{ee}^2\rangle^{1/2}$) to the maximum possible end-to-end distance (or contour length), L_c. Note that L_c for this coarse-grained system corresponds to the maximum extensibility r_m defined in eq 4. Figure 9 shows the dependence of end-to-end distance on elongation ratio for two of the 15−300 bimodal networks and the short chain unimodal network. In the 90 mol % short chain network, the end-to-end distance of both the short and long chains increases with strain. As the chains are increasingly extended, limited extensibility effects play a large role in its improved stress−strain performance, and the load is shared by both types of chains. Unlike the case of the 60 mol % short chain network, the close correspondence of the short chain extension in the 90 mol % short chain network with the pure short chain (100%) network further supports the idea that the short chains are fully elastically coupled in this bimodal network.

The smaller chains in the 60 mol % short chain network, meanwhile, are completely protected from deformation. As shown by the open diamonds in Figure 9, their average end-to-end distance remains virtually unchanged even as α approaches 4. This result reinforces the depiction of bimodal networks with relatively fewer short chains as having a highly heterogeneous structure. The densely cross-linked islands of smaller chains are spared from stretching as only the long chains deform.

The simulation predictions of the order parameter s for both the short and the long chain segments upon extension are shown in Figure 10. The segments of the short chains in the 90 mol % short chain network show the greatest overall alignment and are much more oriented along the strain axis than the segments of the long chains. However, in the 60 mol % network the short and long chains align almost to the same degree with strain. These results suggest that the short chains are much more protected from deformation when they are clustered than when within a more percolated homogeneous network. The short chain segments are subjected to the mean field imposed by the deformation of the long chains and exhibit the same orientation behavior. At the length scale of end-to-end distance, the extension of the two types of chains is different

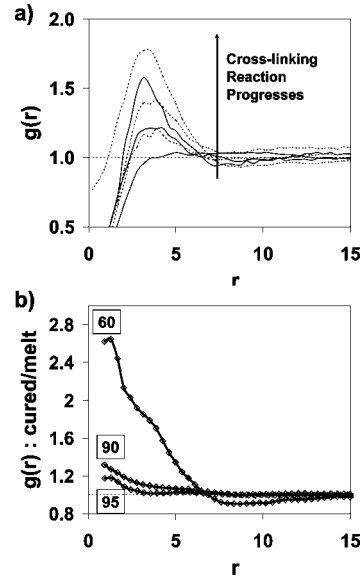

Figure 8. (a) $g(r)$ vs r in units of bead diameters for short chain centers of mass in the 60 mol % short chain 15−300 network at six instances during the cross-linking reaction (alternate instances in dashed lines). (b) $g(r)_{network}/g(r)_{precursor}$ vs r for 15−300 networks. Curves are labeled with mol % short chains.

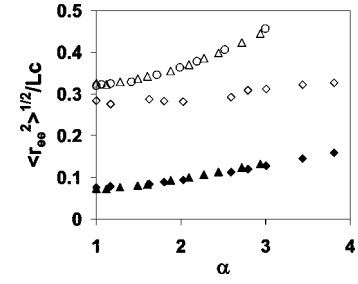

Figure 9. $\langle r_{ee}^2\rangle^{1/2}/L_c$ vs α for the 60 mol % short (diamonds), 90 mol % short (triangles), and 100 mol % short chain (circles) 15/300 network. Short chain data are represented by open symbols, while long chain trends use filled symbols. These simulations do not model network fracture.

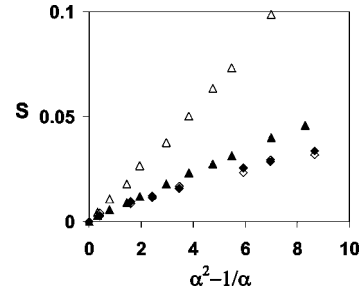

Figure 10. S vs $\alpha^2 - \alpha^{-1}$ for the 60 (diamonds) and 90 mol % (triangles) short chain 15−300 networks. Short chain data are represented by open symbols, while long chain trends use filled symbols.

as is shown in Figure 9. This difference in behavior of segment orientation and end-to-end distance is due to the different length scales examined and has been demonstrated previously.[54] The increase in the segmental orientation in the 90 mol % short chain network is likely due to the ability of the long chains to transfer their load onto the short chains, which they are unable to do in a structure of short chain clusters.

The increased segment orientation of both short and long chains with increasing short chain concentration is consistent with previous deuterium NMR,[55] infrared dichromism,[56] and Monte Carlo[57] studies on bimodal networks. This is not

surprising as ideal rubber elasticity predicts S to be proportional to the modulus which increases with short chain concentration.

5.2.3. Networks Defects. In simulations of topologies in bimodal networks, von Lockette and Arruda[58] found a large extent of loop formation of short chains. We examine here two types of imperfections: single loops and pendant material. A single loop is a chain that has its two ends connected to the same cross-linker. On the other hand, if there is only one path from any network terminal point (i.e., loops, end-capped, and dangling chains) to the rest of the network, all chains belonging to that path are considered pendant material. Chains that are not loops or pendant are said to be part of the elastic material. The amount of elastic material is, however, slightly overestimated because there are some other types of network imperfections that were not taken into account in this work (e.g., loops with more than one chain). Based on these definitions, the network topological characterization for the 15−300 series is shown in Table 4. In general, for the simulated bimodal networks (short chains content ranging from 60% to 95%), the amount of loops and pendant material in the network increases as the content of short chains decreases. When we analyzed long chains alone, almost no long chain loops were observed, and just a small percentage of them (i.e., from 2% to 8%) were pendant. On the contrary, while the amount of pendant material in the short chains does not vary significantly (staying around 2%) with the content of short chains, the percentage of short chain loops does increase significantly (i.e., from 5% to 32%).

Since the important variables for the loop-forming process are the cross-linker density (ρ_x) and the volume that the chain ends can explore (e.g., the chain ends pervaded volume $\sim \langle r_{ee}^2\rangle^{3/2}$), a convenient dimensionless quantity to characterize the proclivity to loop formation is $n_x = \rho_x\langle r_{ee}^2\rangle^{3/2}$ which is a measure of the number of cross-linkers accessible to a given chain end. Thus, the higher n_x is, the higher the probability of a chain end of finding another cross-linker (i.e., different from the one attached to the other chain end) and not forming a loop. The n_x values were calculated for long and short chains in the 15−300 network series and are shown in Table 4. For the long chains $n_x \gg 1$ in all networks, which explains why these chains do not form loops. Conversely, for the short chains $n_x \sim O(1)$ or $n_x < 1$, indicating a significant probability that the ends of a given chain will attach to the same cross-linker.

Figures 11 shows how the short chain end-to-end distance (r_{ee}, in units of bead diameters) distributions evolve upon deformation of the networks with 90 and 60 mol % of short chains. For both networks, the early bumps in the short chain r_{ee} distributions, which correspond to the short chain loops, do not shift to the right in any of the cases. This is because the r_{ee} of looped chains cannot be greater than two chain segments (2.4 in our model). Additionally, and as expected from Figure 9, the second hump (representing mostly elastic chains) of the short chain r_{ee} distribution of the 90 mol % system shifts with deformation considerably more to the right than the short chain r_{ee} distribution of the 60 mol % network. This behavior of the short chains in the 60 mol % network can be attributed to their stronger clustering.

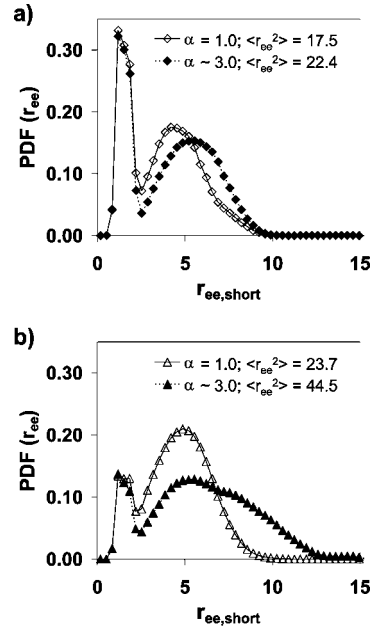

Figure 11. Short chains end-to-end distance probability density functions for the systems with (a) 60 mol % (diamonds) and (b) 90 mol % (triangles) of short chains at $\alpha = 1.0$ (unperturbed state, empty symbols) and $\alpha = 3.0$ (deformed state, solid symbols).

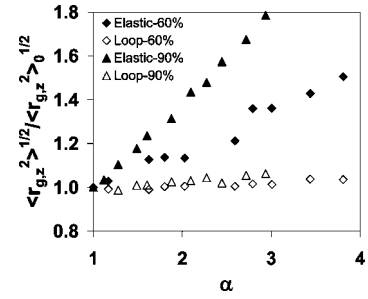

Figure 12. Chain extension ratio (relative to unperturbed state) versus macroscopic extension ratio for the elastic (solid symbols) and looped (empty symbols) short chains in the 60 mol % (diamonds) and 90 mol % (triangles) networks.

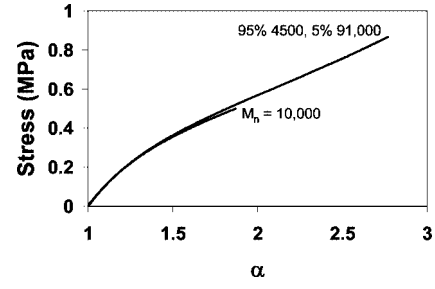

Figure 13. Stress−elongation ratio curves for a 4500−91 000 M_n bimodal network and a "equivalent" unimodal network of 10 000 g/mol.

Table 4. Characterization of the Simulated 15−300 Network Series

		network topological characterization (mol %)			short chains topological characterization (mol %)			long chains topological characterization (mol %)			n_x	
short chain content (mol %)	w_{sol} (mass%)	loops	pendant	elastic	loops	pendant	elastic	loops	pendant	elastic	short chains	long chains
100	0.34	5.1	2.5	92.3	5.1	2.5	92.3				3.0	
95	0.00	7.6	1.6	90.8	8.0	1.5	90.5	0.0	2.4	97.6	1.6	197
90	0.00	11.0	1.7	87.3	12.2	1.8	85.9	0.0	0.0	100.0	1.1	127
60	0.07	19.7	4.4	76.0	31.8	1.8	66.4	1.4	8.2	90.4	0.4	47
0	0.00	0.0	1.3	98.8				0.0	1.3	98.8		21

Table 5. Bimodal vs Unimodal Network Properties

M_n of short chains	M_n of long chains	mol %, mass % of short chains	M_{avg}	E (MPa)	Q	cross-link $\rho \times 10^3$ (mol xlink/g PDMS)	toughness (MPa)	ultimate stress (MPa)
4 500	91 000	95, 48	8 830	1.09 ± 0.03	3.40	0.034	0.79 ± 0.09	0.82 ± 0.04
10 000	(unimodal)	100	10 000	1.04 ± 0.03	3.16	0.030	0.20 ± 0.06	0.44 ± 0.06

In order to determine whether short chain loops contribute directly to the elasticity of the network by forming trapped "entanglements", we monitored the deformation response for loops, elastic, and pendant short chains separately. Figure 12 shows the normalized component of the radius of gyration along the strain axis—which can be interpreted as a microscopic extension ratio for the short chains—versus the extension ratio. From this figure we can conclude that short chain loops barely deform when the network is stretched, even for the 90 mol % system (where most of the short chains are fully elastically coupled). Hence, the contribution of short chain loops to the network elasticity seems to be insignificant. Additionally, any cross-linker that has a loop can at most have two connected elastic chains causing them behave as a single, effectively larger elastic chain; this implies that there is an additional loss of at least one elastic chain for every loop formed. Note, however, that the artificial bulkiness of our bead-based short chain model makes it difficult for the short chains to loop around other chains to form trapped "entanglements" that would contribute to the elasticity of the network. The detrimental effect of loop formation on the elastic properties of hydrogels was recently documented,[59] where inelastic loop formation was favored by the high dilution at which network formation took place.

5.3. Comparison to "Equivalent" Unimodal Networks. While we have shown improved mechanical properties in bimodal networks when compared to the corresponding pure short chain and long chain networks, it is perhaps more appropriate to weigh their performance against more similar unimodal networks. Such a comparison requires unimodal and bimodal networks with similar cross-link densities. For networks with equivalent values of r, defined following eq 2, similar cross-link density also means similar average molar mass. M_{avg} of a bimodal network is easily calculated from the molar fractions of the short and long chains and their respective molar masses:

$$M_{avg} = x_{short}M_{n,short} + x_{long}M_{n,long} \quad (9)$$

Comparisons of a unimodal network to a bimodal network of similar average molar mass and cross-link density are shown in Table 5 and Figure 13. From the figure, it is easily seen that the two networks have almost identical stress−strain behavior in the region $\alpha < 2$. However, whereas the unimodal network broke before it reached twice its initial length, the bimodal network stretched much further before fracture, exhibits a stress upturn as discussed earlier, and shows greatly improved toughness and ultimate stress (Table 5). Thus, it is clear that the synergistic effect gained via bimodality manifests itself in improved high-strain properties rather than equilibrium modulus.

6. Conclusions

Mechanical and swelling properties of PDMS bimodal networks were obtained and compared with Monte Carlo simulations. While improvements in mechanical properties were previously demonstrated with non-Gaussian short chains on order of 1000 g/mol, we find that networks with Gaussian short chains in their unperturbed states also showed enhancement in properties. We examined two prevalent hypotheses for the nature of the improvement in ultimate mechanical properties. While short chains will cluster at lower mol % of short chains (typically below their overlap concentration), these networks do not show increased toughness or upturns in stress. Instead, it appears that the finite extensibility of the short chains at high strain ratios plays a significant role in ultimate property improvement and occurs only at fairly high molar concentrations of short chains where the short chains are intimately coupled to the long chains and the load is distributed among both types of chains. The best performing bimodals in terms of stored, strain energy at break may still have some residual short chain clusters that are shielded by the long chains from stress overload. This allows the network to sustain high elongation before the short chains are stressed to their breaking point.

Combining results from experiments and simulations allows us to propose a possible mechanism for the molecular level deformation of the end-linked chains in quasi-homogeneous bimodal networks. The physical picture that emerges is that the toughest networks have their short and long chains intimately coupled. Most chains are stretched initially, resulting in a modulus between that of a pure long chain and a pure short chain network. Then, just as in unimodal networks, the bimodal networks begin to deviate from the model of ideal rubber elasticity as trapped entanglements slip and interacting chains are pulled apart. Eventually, the short chains begin to stretch significantly and the large forces required to deform them further result in an upturn in stress in the stress−elongation curves. While an equivalent unimodal network would have broken earlier, the presence of the long chains allows the bimodal systems to stretch further before fracture. We are planning and pursuing further molecular level tests of the physical picture presented here using D-NMR and neutron scattering measurements.

Acknowledgment. This work was supported by the National Science Foundation Polymers Program under grants DMR-0349952 and DMR-0705565. This work also made use of the Cornell Center for Materials Research Shared Experimental Facilities supported through the National Science Foundation Materials Research Science and Engineering Centers program (Award DMR-0079992).

Supporting Information Available: Figures for the simulated 4−69 bead results which were omitted for space considerations; comparison with the experimental stress−strain curves of the 800−21 000 g/mol bimodal network as well as the cluster formation (analogue of Figure 8) in this system. This material is available free of charge via the Internet at http://pubs.acs.org.

References and Notes

(1) Andrady, A. L.; Llorente, M. A.; Mark, J. E. *J. Chem. Phys.* **1980**, *72*, 2282–2290.
(2) Patel, S. K.; Malone, S.; Cohen, C.; Gillmor, J.; Colby, R. *Macromolecules* **1992**, *25*, 5241–5251.
(3) Valles, E. M.; Macosko, C. W. *Macromolecules* **1979**, *12*, 673–679.
(4) Meyers, K. O.; Bye, M. L.; Merrill, E. W. *Macromolecules* **1980**, *13*, 1045–1053.
(5) Sivasailam, K.; Cohen, C. *J. Rheol.* **2000**, *44*, 897–915.
(6) Urayama, K.; Kohjiya, S. *Polymer* **1997**, *38*, 955–962.
(7) Kawamura, T.; Urayama, K.; Kohjiya, S. *J. Polym. Sci., Polym. Phys.* **2002**, *40*, 2780–2790.
(8) Chen, Z.; Cohen, C.; Escobedo, F. A. *Macromolecules* **2002**, *35*, 3296–3305.
(9) Stepto, R. F. T.; Taylor, D. J. R. *J. Chem. Soc., Faraday Trans.* **1995**, *91*, 2639–2647.
(10) Stepto, R. F. T.; Cail, J. I.; Taylor, D. J. R. *Mater. Res. Innovations* **2003**, *7*, 4–9.

(11) Llorente, M. A.; Andrady, A. L.; Mark, J. E. *J. Polym. Sci., Polym. Phys.* **1981**, *19*, 621–630.
(12) Mark, J. E.; Tang, M.-Y. *J. Polym. Sci., Polym. Phys.* **1984**, *22*, 1849–1855.
(13) Wu, W. L.; Jong, L.; Hanyu, A.; Coyne, L. D.; Stein, R. S. *Macromolecules* **1990**, *23*, 351–353.
(14) Hecht, A.-M.; Horkay, F.; Geissler, E. *J. Phys. Chem. B* **2001**, *105*, 5637–5642.
(15) Subramanian, P. R.; Galiatsatos, V. *Makromol. Chem., Macromol. Symp.* **1993**, *76*, 233–240.
(16) Oikawa, H. *Polymer* **1992**, *33*, 1116–1119.
(17) Saalwachter, K.; Ziegler, P.; Spyckerelle, O.; Haidar, B.; Vidal, A.; Sommer, J.-U. *J. Chem. Phys.* **2003**, *119*, 3468–3482.
(18) Smith, T. L.; Haidar, B.; Hedrick, J. L. *Rubber Chem. Technol.* **1990**, *63*, 256–264.
(19) Mark, J. E.; Curro, J. G. *J. Chem. Phys.* **1983**, *79*, 5705–5709.
(20) Curro, J. G.; Mark, J. E. *J. Chem. Phys.* **1984**, *80*, 4521–4525.
(21) Llorente, M. A.; Rubio, A. M.; Freire, J. J. *Macromolecules* **1984**, *17*, 2307–2315.
(22) Erman, B.; Mark, J. E. *J. Chem. Phys.* **1988**, *89*, 3314–3316.
(23) Zhang, L.-X.; Jiang, Z.-T.; Zhao, D.-L. *J. Polym. Sci., Polym. Phys.* **2002**, *40*, 105–114.
(24) von Lockette, P. R.; Arruda, E. M.; Wang, Y. *Macromolecules* **2002**, *35*, 7100–7109.
(25) Lee, C. L.; Johannson, O. K. *J. Polym. Sci., Polym. Chem.* **1976**, *14*, 729–742.
(26) Lee, C. L.; Marko, O. W.; Johannson, O. K. *J. Polym. Sci., Polym. Chem.* **1976**, *14*, 743–758.
(27) Lapp, A.; Herz, J.; Strazielle, C. *Makromol. Chem.* **1985**, *186*, 1919–1934.
(28) Takahashi, H.; Shibyama, M.; Fujisawa, H.; Noruma, S. *Macromolecules* **1995**, *28*, 8824–8828.
(29) Carmesin, I.; Kremer, K. *Macromolecules* **1988**, *21*, 2819–2823.
(30) Deutsch, H.-P.; Binder, K. *J. Chem. Phys.* **1991**, *94*, 2294–2304.
(31) Binder, K.; Paul, W. *J. Polym. Sci., Polym. Phys.* **1997**, *35*, 1–31.
(32) Gilra, N.; Cohen, C.; Panagiotopoulos, A. Z. *J. Chem. Phys.* **2000**, *112*, 6910–6916.
(33) Bhawe, D. M.; Cohen, C.; Escobedo, F. A. *Macromolecules* **2004**, *37*, 3924–3933.
(34) Trautenberg, H. L.; Sommer, J.-U.; Goritz, D. *J. Chem. Soc., Faraday Trans.* **1995**, *91*, 2649–2653.
(35) Trautenberg, H. L.; Sommer, J.-U.; Goritz, D. *Macromol. Symp.* **1994**, *81*, 153–160.
(36) Paul, W.; Binder, K.; Heermann, D.; Kremer, K. *J. Phys. II* **1991**, *1*, 37–60.
(37) Meissner, B.; Matejka, L. *Polymer* **2005**, *46*, 10618–10625.
(38) Escobedo, F. A.; de Pablo, J. J. *J. Chem. Phys.* **1997**, *106*, 793–810.
(39) Rivlin, R. S.; Thomas, A. G. *J. Polym. Sci.* **1953**, *10*, 291–318.
(40) Genesky, G. D.; Cohen, C.; Krishnan, V.; Hui, C.-Y. Manuscript in preparation.
(41) Flory, P. J. *Statistical Mechanics of Chain Molecules*; Interscience: New York, 1969.
(42) Flory, P. J. *Principles of Polymer Chemistry*; Cornell University Press: Ithaca, NY, 1953.
(43) Mooney, M. *J. Appl. Phys.* **1940**, *11*, 582–592.
(44) Rivlin, R. S. *Philos. Trans. R. Soc.* **1948**, *A241*, 379–397.
(45) Treloar, L. R. G. *The Physics of Rubber Elasticity*, 3rd ed.; Clarendon Press: Oxford, 2005.
(46) Morris, M. C. *J. Appl. Polym. Sci.* **1964**, *8*, 545–553.
(47) Meissner, B. *Polymer* **2000**, *41*, 7827–7841.
(48) Mark, J. E. In *Physical Properties of Polymers*, 2nd ed.; American Chemical Society: Washington, DC, 1993.
(49) Putz, M.; Kremer, K.; Grest, G. S. *Europhys. Lett.* **2000**, *49*, 735–741.
(50) Sides, S. W.; Curro, J.; Grest, G. S.; Stevens, M. J.; Soddemann, T.; Habenschuss, A.; Londono, J. D. *Macromolecules* **2002**, *35*, 6455–6465.
(51) Lide, D. R. In *CRC Handbook of Chemistry and Physics*, 87th ed.; CRC Press: Boca Raton, FL, 2006; pp 9−46.
(52) Weiss, P.; Herz, J.; Rempp, P. *Makromol. Chem.* **1970**, *135*, 249–261.
(53) Sommer, J.-U.; Lay, S. *Macromolecules* **2002**, *35*, 9832–9843.
(54) Gilra, N.; Cohen, C.; Briber, R. M.; Bauer, B. J.; Hedden, R. C.; Panagiotopoulos, A. Z. *Macromolecules* **2001**, *34*, 7773–7782.
(55) Chapellier, B.; Deloche, B.; Oeser, R. *J. Phys. II* **1993**, *3*, 1619–1631.
(56) Besbes, S.; Bokobza, L.; Monnerie, L.; Bahar, I.; Erman, B. *Macromolecules* **1995**, *28*, 231–235.
(57) Sotta, P. *Macromolecules* **1998**, *31*, 8417–8422.
(58) Von Lockette, P. R.; Arruda, E. M. *Macromolecules* **1999**, *32*, 1990–1999.
(59) Shen, W.; Kornfield, J. A.; Tirrell, D. A. *Soft Matter* **2007**, *3*, 99–107.

MA801065X